THE JOURNAL OF PHYSICAL CHEMISTRY C

Subscriber access provided by UNIV OF WISCONSIN - MADISON

C: Physical Processes in Nanomaterials and Nanostructures

Adsorption Dynamics and Structure of Polycations on Citrate-Coated Gold Nanoparticles

Gene Chong, and Rigoberto Hernandez

J. Phys. Chem. C, **Just Accepted Manuscript** • DOI: 10.1021/acs.jpcc.8b05202 • Publication Date (Web): 01 Aug 2018

ACS Publications

is published by the American Chemical Society. 1155 Sixteenth Street N.W., Washington, DC 20036

Adsorption Dynamics and Structure of Polycations on Citrate-Coated Gold Nanoparticles

*Gene Chong and Rigoberto Hernandez**

Department of Chemistry, Johns Hopkins University, Baltimore, Maryland 21218, United States

ABSTRACT

Despite the widespread application of engineered multilayered polyelectrolyte-coated gold nanoparticles (AuNPs), their interparticle interaction is not fully understood in part because of a lack of molecular scale observation of the layer-by-layer assembly of the polyelectrolyte coating. While top-down coarse-grained models of polyelectrolyte-coated AuNPs have focused on polyelectrolytes of short length—from ten to a hundred monomers represented as one charged bead per monomer—here we use molecular dynamics and bottom-up coarse-grained approaches to access more typical polymer lengths on the order of two hundred monomers. Specifically, we simulate the adsorption dynamics and structure of one or two such long polycations on negatively charged 4-nm citrate-coated AuNPs within implicit or explicit solvents. The first polycation coats approximately half of the AuNP surface regardless of solvent model, and leaves a significant part of the anionic citrate layer exposed to absorption by a second polycation. We find that the most prevalent structural features across solvent conditions consist of 1-2 monomer loops, or kinks. They extend radially from the nanoparticle surface and assemble into a double-

layered coating of the AuNP. We compile a set of structural features of adsorbed polycations that would be ripe for coarse-graining and outline a bottom-up coarse-graining scheme for simulations of polyelectrolyte-coated AuNPs with amphiphilic biomolecules that incorporates the hemispheric polycation coverage with exposed citrate layer, surface-bound bilayer-like segments, and long amphiphilic loops and tails.

I. Introduction

Gold nanoparticles (AuNPs) have promising biomedical applications due to their tunable shape, size, and surface chemistry.[1] In particular, layer-by-layer assembly of oppositely charged polyelectrolytes onto the AuNP surface with molecular probes or small drug molecules embedded between layers allows for AuNPs to act as sensing,[2] imaging,[3] and drug-delivering agents.[4,5] Controlled grafting of other ligand types, such as alkanethiols, organic linkers, and reactive polymers into Janus or multi-striped patterns on the nanoparticle surface can also promote the self-assembly of these engineered nanoparticles into unique architectures with self-healing properties.[6-8] In addition to exhibiting a desired function or property, such particles increasingly must satisfy an additional figure of merit: they and their transformations in the environment must have zero or minimal impact on biological systems.[9,10] As an example, AuNPs grafted with charged, long-chained alkanethiols have been seen in simulations to insert into and disrupt lipid membranes,[11-15] AuNPs coated with the cationic polyelectrolyte poly(allylamine hydrochloride) (PAH) are more prone to aggregation compared to alkanethiol-coated AuNPs despite having a higher surface charge density.[16] PAH-coated AuNPs (PAH-AuNPs) have also been shown to bind irreversibly to supported lipid bilayers[17] and exhibit greater toxicity to

bacteria[16] and simple multicellular organisms.[18,19] A better understanding of the polyelectrolyte-nanoparticle interface is therefore required to control the interactions of nanoparticles in the environment and, thereby, nanoparticle functionality and possible toxicity.

Computer simulations can potentially link atomistic-scale interactions between nanoparticles and biomolecules to the onset of toxicity in cells but require accurate bottom-up coarse-graining to tackle this inherently multiscale problem.[20,21] A common bottom-up coarse-graining strategy for complex multi-component systems, such as nanoparticles in suspension media or in biological environments, starts with the atomistic structure of each component at the lowest scale, and then groups neighboring atoms with similar chemical properties into larger beads at the higher scale. The MARTINI coarse-grained lipid model[22] follows a similar approach and has been parameterized by Marrink and co-workers to obtain a force field[23] that can reproduce the partitioning of polar and apolar phases across a broad class of amphiphilic molecules. The MARTINI force field has also been used to study the aggregation[24] of AuNPs coated with alkanethiols of different length and terminal groups and the interaction between lipid bilayers and alkanethiol-coated nanoparticles that were first constructed using atomistic molecular dynamics simulations and subsequently coarse-grained.[25] Polymers, such as polystyrene of up to 100 monomers, have also been rigorously parameterized bottom-up[26] with the MARTINI force field. For polyelectrolyte-coated nanoparticles, many computational studies have focused largely on top-down models of polyelectrolytes of relatively short length, ranging from tens of monomers to a hundred, in which monomers are represented as single charged beads. Molecular dynamics simulations of top-down polyelectrolyte models have been used to characterize polyelectrolyte adsorption onto flat[27] and spherical surfaces.[28,29] These simulations have shown that highly charged polyelectrolytes localize charge by distributing into multiple

layers through the formation of loops and tails. Loops consist of free, solvent-exposed segments of polymers flanked by surface-bound segments referred to as trains. Tails form if the ends of the polymer are free instead of surface-bound. Nuclear magnetic resonance (NMR) spectroscopy of the polyelectrolyte PAH covalently grafted onto 5-nm nanodiamond similarly reveal both motion-restricted regions of PAH bound to the surface and highly mobile ones, suggesting the presence of loops and tails that extend into solution.[30] The heterogeneous spatial distribution of dynamic charged groups in polyelectrolyte-coated AuNPs could be a factor in why polyelectrolyte-coated AuNPs induce larger biological responses than alkanethiol-coated AuNPs.

Here, we perform atomistic molecular dynamics simulations of polyelectrolyte adsorption onto AuNPs to reveal other chemical properties at the atomistic level in addition to charge distribution that need to be represented in coarse-grained models. A combination of implicit- and explicit-solvent simulations is used to study the adsorption dynamics, surface coverage, and structure of PAH on AuNPs. Specifically, we deposit PAH such that the end-to-end vector of the polyelectrolyte is normal to the AuNP surface. We observe the relaxation and equilibrium behavior of a finite number of trajectories of this system, both in implicit and explicit solvents. While the set is not enough to have complete representation of the ensemble, this finite poll exhibits a range of behaviors providing a view of the end-to-end adsorption and resulting structure of longer-length polyelectrolytes on AuNPs. Geiger and co-workers determined that the average number of ammonium groups per PAH adsorbed onto 4-nm citrate-coated AuNPs is 200.[31] We therefore deposit PAH of 200 monomers (PAH_{200}) on a 4-nm citrate-coated AuNP in simulations. Although both experiment and simulation have shown preferential binding of ligands —specifically citrate and poly(vinylpyrrolidone) (PVP)— on different facets of gold[32] and silver nanoparticles,[33,34] respectively, here we study the simpler case of a homogeneously

covered citrate-coated AuNP along with fully protonated PAH_{200} (Fig. 1). Both experimental and computational studies[35,36] have also shown that protonation levels of PAH can vary from 0.14 in neutral pH solution to 0.70 at charged lipid-membrane interfaces due to local pH effects. The use of a fully protonated PAH_{200} in our all-atom model allows for direct comparison to top-down, coarse-grained models of fully charged polyelectrolytes and serves as a benchmark for future coarse-grained simulations investigating how variation in protonation states and sites along longer-length polyelectrolytes affects polyelectrolyte conformation and surface coverage on AuNPs. Further, the results are useful in identifying reduced-dimensional variables and observables that would be relevant for a new bottom-up coarse-grained approach for polyelectrolyte-coated AuNPs of possible use in simulating both the polyelectrolyte-AuNP interface and the nano-bio interface.

In this paper, we report the development of our all-atom 4-nm PAH-AuNP model from the construction of a 4-nm AuNP, and the adsorption of the negatively-charged citrate layer to the adsorption of the polycation layer in Section II. Despite different adsorption dynamics shown in Sec. III A, longer-length polycation PAH_{200} conformations cover approximately half of the 4-nm AuNP surface, leaving the citrate layer exposed (Sec. III B). The hydrophilic charged groups of PAH_{200} segregate radially relative to the AuNP center into multiple layers due to the competition between electrostatic attraction to the AuNP surface and repulsion between monomers (Sec. III C). We reproduce the formation of solvent-exposed loops and tails and surface-bound trains observed in top-down models.[27-29] At the atomistic scale, we find that short 1-2 monomer trains and loops are the dominant structural features of the adsorbed PAH_{200}, forming bilayer-like segments on the AuNP surface (Sec. III D). We conclude with a possible coarse-graining scheme described in Sec. III E, incorporating the hemispheric coverage of the

polycation with exposed citrate layer, surface-bound bilayer-like segments, and dynamic amphiphilic loops and tails unique to PAH-AuNPs. For coarse-grained simulations of the nano-bio interface, we find that it would be essential and appropriate to implement this minimum level of detail for interactions of these polyelectrolyte-coated nanoparticles with amphiphilic biomolecules, such as lipids and proteins.

II. Materials and Methods

A. Citrate-coated AuNP, PAH_{200}, and Solvent Models

AuNPs were created by placing gold atoms two atomic radii apart, arranged in a face-centered cubic lattice contained within a sphere, and equilibrating at 300 K in vacuum, using Lennard-Jones parameters developed by Heinz and co-workers[37] to create a nearly spherical, 4-nm-diameter multifaceted core. In simulations for the adsorption of citrate and PAH_{200} onto gold, a shallower potential-well depth is used for the Lennard-Jones parameter, ε, for gold,[38,39] and positions of gold atoms are kept fixed throughout the simulations. The OPLS-UA force field[40] was used for the carbon backbones of citrate and PAH_{200} and the -AA force field[41] for charged terminal groups, sodium and chloride counterions, and TIP3P solvent. The list of force-field parameters is presented in Table S1 (Supporting Information).

Citrate-coated AuNPs were constructed in implicit solvent. Implicit solvent for all simulations was modeled using a Langevin thermostat at 300 K, a damping constant of 10 ps^{-1}, relative permittivity of 80.1, and the particle-particle particle-mesh (PPPM) method to compute electrostatic interactions in the presence of explicit counterions. Following the surface citrate density predicted by experiment[32] and used in simulations,[42] we randomly distributed 90 $citrate^{3-}$ molecules in a simulation box with the AuNP at the center. A steering force was applied to guide the central carboxylate groups of citrate molecules to the AuNP surface. We focus on the

citrate^{3-} charge state, although the presence of H_2citrate$^-$ on the AuNP surface has also been reported.[32] The effect of citrate charge state on polycation adsorption will be discussed in a future article. Due to the known unphysical electrostatic interactions between the hydroxyl hydrogen and central-carboxylate oxygen in citrate that occur with existing force fields,[43] the citrate backbone that contains the central carboxylate and hydroxyl groups was kept rigid and fixed on the AuNP surface for subsequent simulations. At charged interfaces, it is possible that small charged molecules reorient or detach from the interface, as observed at the lipid-water interface upon adsorption of polycations.[44] In studies of protein adsorption onto citrate-coated AuNPs, the use of AuNP models with citrate fixed on the surface in simulations has been seen to lead to final protein orientation on the AuNP surface in agreement with experiment.[42,45]

PAH_{200} was initially fully extended and energy minimized. The atoms were given random initial velocities and heated to 300 K in implicit solvent, until the PAH_{200} reached a random-coil state that fit in a 200 × 100 × 100 Å water box. PAH_{200} was equilibrated for 50 ns in TIP3P water with chloride ions. All explicit-solvent simulations were run at constant NPT at 1.0 atm and 300 K with a 1.0-fs timestep, using the PPPM method for electrostatic calculations. Five different PAH_{200} conformations were generated using this setup, which reproduced loosely clustered regions along the extended polymeric backbone as previously observed in simulations of polyelectrolytes in explicitly modeled poor solvent (*eg.* water).[46] Each conformation was paired with a different citrate-coated AuNP in simulations (Figure S1, Supporting Information).

B. Methods: All-Atom Simulations

The adsorption of PAH_{200} onto citrate-coated AuNPs was simulated using both implicit- and explicit-solvent conditions. Periodic boundary conditions are used with at least 15 Å from the PAH_{200} and AuNP to the edges of the simulation box along x, y, and z dimensions. Box sizes

were chosen such that the salt concentration fell within the range 0.1-0.2 M with varying number of PAH_{200} added and the changing box size during the NPT equilibration. Box volumes were approximately 5×10^6 Å^3 and included ~500,000 atoms in explicit-solvent simulations. Initial configurations for all simulations were generated using Packmol,[47] and all simulations were performed using LAMMPS[48] at 1.0 fs per timestep with 10-Å cutoff for pairwise interactions. On the XSEDE HPC resource Bridges, this required ~480 CPU hours to integrate for 120 ns on 448 processors, and this limited the number of trajectories that were obtained. Additional simulation details on system size and simulation times are in Table S2 in the Supporting Information.

For implicit-solvent simulations, PAH_{200} was initially equilibrated in explicit solvent along with its coordinating chloride ions and then placed near a nanoparticle with one of the polycation's ends 8 Å away from its surface (Fig. 1). Sodium and chloride ions were allowed to equilibrate for 2.5 ns, while keeping the atoms in the gold core and PAH_{200} fixed. The constraints on PAH_{200} were removed, and the distances between each nitrogen atom per monomer of PAH_{200} and the nanoparticle's center of mass (NP-COM) were tracked at each timestep to check the progress of PAH_{200} adsorption. Once all nitrogen atoms were within 4 nm of the NP-COM, simulations were run for an additional 5 ns with data collected every picosecond during the last nanosecond. Five simulations were run in total—one for each PAH_{200} conformation. An additional simulation was run for each condition so as to observe the deposition of a second PAH_{200} onto the opposite pole from which the first was added.

For explicit-solvent simulations, the PAH_{200} was placed near the AuNP with one of the polycation's ends at 4 Å away from its surface. The gold core and PAH_{200} were first fixed, and water and counterions were allowed to equilibrate for 0.5 ns. To track adsorption of PAH_{200} once released, each PAH_{200} was evenly divided into five segments, and the distances between the

COM of the first, middle, and last 40-monomer segments—labelled 1, 3, and 5, respectively—and their NP-COMs were plotted over time (Figure 2). These distances relaxed to a small constant value after 110 ns of simulations, signifying adsorption. Simulations were then run for an additional 10 ns with data collected every 10 ps.

Due to the system size, three simulations were run in explicit solvent. We compare the adsorption of the three starting configurations for PAH_{200} used in both implicit- and explicit-solvent simulations. Results for the remaining two PAH_{200} conformations used in implicit-solvent simulations are presented in the Supporting Information. From this finite number of trajectories, we find common structural features that emerge upon adsorption of long-length polyelectrolytes onto the AuNP surface independent of solvent condition.

C. Methods: Coarse-Graining Schemes

From the final frame of each simulation run in explicit solvent, we group the three-carbon chain into one hydrophobic bead and the ammonium group into one charged bead for each monomer with bead positions set by their centers of mass. We provide a preliminary coarse-graining scheme to emphasize atomistic properties that will be implemented in future coarse-grained simulations of PAH-AuNPs at the interface of biomembranes. The coarse-grained structures are therefore a product of the all-atom simulations of this work, and are available for use in coarse-grained simulations in future work.

III. Results and Discussion

A. Adsorption dynamics of PAH_{200}.

The effect of implicit and explicit solvent on dynamical processes, such as the mechanical pulling of polypeptides,[49] the formation of polyelectrolyte complexes,[50] and the adsorption of polyelectrolytes onto surfaces,[51,52] has been well addressed. For the dynamical behavior of the

system, we, therefore, focus our attention on the differences in adsorption dynamics in explicit solvent between different starting PAH_{200} conformations. For each simulation, PAH_{200} was initially aligned such that the end-to-end vector was normal to the nanoparticle surface. Figure 2a shows that the first and last 40-monomer segments of PAH_{200} (segments 1 and 5, respectively) adsorb to the surface within 20 ns of each other, leaving the middle 40-monomer segment 3 as a loop in solution. For a different PAH_{200} conformation, segment 3 adsorbs onto the nanoparticle surface first, followed by segment 1 and, then, segment 5 (Figure 2b). Figure 2c shows sequential wrapping of the nanoparticle from segments 1 to 5 by PAH_{200}. Even though the same orientation is used for the initial deposition of PAH_{200} on the nanoparticle surface, different adsorption dynamics are sampled as a result of the different starting conformations of PAH_{200}.

B. Surface coverage of PAH_{200}.

Despite the different adsorption mechanisms per PAH_{200} configuration, PAH_{200} adsorption leads to a half-coated AuNP in all cases (Figure 3). To depict the surface coverage of PAH_{200} on AuNPs, each PAH-AuNP is, first, rotated so that the vector connecting the nanoparticle's center of mass (NP-COM) to the center of mass of PAH_{200} maps onto the positive z-axis. We create a two-dimensional histogram with a bin size of $\pi/20$ radians and track the projection of nitrogen atoms in PAH_{200} onto the AuNP surface as a function of spherical azimuthal- and polar-angle coordinates. The density profile of the nitrogen atoms in PAH_{200} shows that PAH_{200} is more evenly distributed on a hemisphere of the nanoparticle in implicit solvent, whereas more voids are present in the density profiles in explicit solvent, signifying incomplete hemispheric coverage of PAH_{200} (Figure 3). The voids in the surface coverage of PAH_{200} in explicit solvent suggest that there is a greater distribution of monomers along the radial direction relative to the NP-COM arranged in loops exposed to solution.

Incomplete hemispheric coverage of PAH_{200} suggests that a second PAH_{200} could potentially adsorb onto the bottom hemisphere. Due to the system size and computational cost, we limit simulations of a second PAH_{200} adsorption to implicit solvent. These simulations suggest that, in implicit solvent, adsorption of a second PAH_{200} is possible with similar structure to the first adsorbed PAH_{200}. Without the uniform dielectric screening used for our implicit-solvent model, it is possible that the second PAH_{200} incompletely adsorbs enabling the bridging between two AuNPs and promoting the aggregation of 4-nm PAH-AuNPs observed in experiment.[16,31]

C. Radial distribution of PAH_{200}.

The radial distribution function, *g(r)*, between nitrogen atoms of PAH_{200} and the NP-COM is calculated through a histogram —with bin size of 0.1 Å— averaged over 1000 frames per trajectory for five trajectories in implicit solvent and three in explicit solvent, and normalized by the annular volume (Figure 4). The *g(r)*'s for individual trajectories are provided in the Supporting Information. Two major peaks or sets of peaks—one close to the nanoparticle surface (2 nm away from the NP-COM) and another in solution—are present in the *g(r)* from implicit- and explicit-solvent simulations, respectively (Figure 4). After the addition of a second PAH_{200}, the major peaks in the *g(r)* sharpen, but peak positions remain the same. The *g(r)* from explicit-solvent simulations reaches zero by 6-nm from the NP-COM, confirming that PAH_{200} has a broader radial distribution in explicit solvent extending far into solution. The distance between major peaks in the *g(r)* from implicit-solvent simulations is 0.6 nm, which is slightly less than the length of the five-carbon backbone between NH_3^+ groups in adjacent monomers, assuming a carbon-carbon single-bond distance to be 1.54 Å. In addition, the peak heights have the same magnitude, signifying that there is a 1:1 distribution of monomers between the surface-bound

and solvent-exposed layers. These results suggest that the most significant structural features in the addition of PAH_{200} to the NP is the presence of short 1-2–monomer loops and trains— that resemble kinks— extending radially from the NP surface.

D. Structural motifs in PAH_{200}.

To determine the specific structural motifs in PAH_{200} adsorbed onto the NP surface, we perform a histogram count of the number of monomers in solvent-exposed loops, free tails, and surface-bound trains divided by total number of sampled frames. A normalized value greater than 1.0 signifies at least one instance in every frame (Fig. 5). A monomer is considered to be bound to the surface and part of a train if the nitrogen atom is within 3.48 Å from an oxygen atom on citrate; the cutoff distance was chosen to be $2^{1/6}\sigma$ after applying the geometric mixing rule on the nonbonded distance parameter, σ, from the OPLS-AA force field.[41] The solvent-exposed segments within PAH_{200} are considered as loops and free segments at the ends of PAH_{200} as tails. Representative snapshots of loop, tail, and train structures are shown in Figure S2 in the Supporting Information. As suggested from the radial distribution functions, 1-2–monomer, as well as 3–monomer, trains and loops appear most frequently on the nanoparticle surface (Fig. 5). Adsorption of PAH_{200} in implicit solvent leads to a similar distribution of short trains and loops with up to 10-monomers per loop, whereas adsorption in explicit solvent leads to a more varied distribution in loop and tail length.

E. Bottom-up coarse-graining scheme for PAH_{200}-AuNPs.

Despite the heterogeneity in the structure of PAH_{200} on AuNPs, it is important to identify which atomistic properties need to be represented in coarse-grained models of polyelectrolyte-coated AuNPs. From the atomistic PAH_{200}-AuNP structures obtained from explicit-solvent simulations, we construct initial coarse-grained structures for PAH_{200} by grouping the atoms in the carbon

backbone of each monomer and NH_3^+ group into beads positioned at their respective centers of mass. These coarse-grained PAH_{200} structures are shown with the atomistic AuNP core in Fig. 6. Figure 6 highlights the radial extension of charged NH_3^+ groups via small solvent-exposed loops formed between surface-bound trains. The separation of charged groups connected by the carbon backbone within adjacent monomers reveals a bilayer-like motif on the nanoparticle surface. Several groups[11-15] have used simulations of charged alkanethiol-coated AuNPs with lipid bilayers to demonstrate that exposed hydrophobic groups in the alkanethiols are required at the nanoparticle-ligand interface for nanoparticles to associate with and disrupt lipid bilayers. This molecular scale structure on larger scale behavior is important because it is absent in existing top-down polyelectrolyte models.[28,29] A coarse-graining scheme for PAH_{200} coating on the AuNP would have to incorporate elements that can give rise to the bilayer-like segments of PAH_{200} observed on the AuNP surface, and dynamic segments in the form of longer loops and tails with amphiphilicity shown in Fig. 6. How the surface-bound segments and heterogeneous spatial charge and hydrophobic backbone distribution in PAH_{200} adsorbed onto AuNPs induce greater membrane disruption[17] and stress responses in organisms[18,19] compared to charged alkanethiol-coated AuNPs still needs to be addressed.

IV. Conclusion

Using atomistic molecular dynamics simulations, we characterize the adsorption and structure of polycations on a citrate-coated gold nanoparticle, and thereby provide a benchmark for structures of polyelectrolyte-coated gold nanoparticles to be used for coarse-grained simulation techniques, such as the MARTINI force field[23] and dissipative particle dynamics.[53,54] The average length of a PAH polycation was determined by experiment[31] to be 200 monomers. Through simulations, we find that adsorption of a single PAH_{200} leads to incomplete hemispheric coverage of the

polyelectrolyte on a 4-nm AuNP. Incomplete hemispheric coverage of positively-charged PAH and the exposed negatively-charged citrate layer on AuNPs could promote the aggregation of 4-nm PAH-AuNPs observed in experiments[16,31] via bridging nanoparticles by oppositely charged patches or by free PAH in solution.[55] The surface coverage of polyelectrolytes with an average length of 200 monomers as a function of nanoparticle size, therefore, needs to be further considered in the design of nanoparticles as a means of controlling nanoparticle aggregation in suspension.

A detailed structural analysis from our simulations confirms the presence of surface-bound and dynamic polyelectrolyte segments on the nanoparticle surface, as previously reported in top-down coarse-grained simulations of polyelectrolyte adsorption[27-29] and NMR experiments.[30] It further shows the atomistic distribution of the hydrophobic carbon backbone and NH_3^+ charged groups into bilayer-like segments bound to the surface and amphiphilic, dynamic segments, from which we construct a new coarse-grained representation for polyelectrolyte-coated AuNPs. Nanoparticle transformations in suspension with free PAH and in biological environments are thus strongly affected by incomplete nanoparticle coverage by a positively-charged polycation, exposed negatively-charged citrate patches, the distribution of polyelectrolyte segments with different dynamics on the surface, and the amphiphilicity of these segments.

ASSOCIATED CONTENT

Supporting Information. Force-field parameters, initial configurations, additional figures from individual trajectories. This material is available free of charge via the Internet at http://pubs.acs.org.

AUTHOR INFORMATION

Corresponding Author

Rigoberto Hernandez, Department of Chemistry, Johns Hopkins University, Baltimore, MD 21218; r.hernandez@jhu.edu

Author Contributions

The manuscript was written through contributions of all authors. Chong carried out the numerical simulations. All authors have given approval to the final version of the manuscript.

ACKNOWLEDGMENTS

The work has been supported by a grant from the National Science Foundation CHE-1503408. Computing resources were provided in part by the National Science Foundation through XSEDE resources under grant number CTS090079.

REFERENCES

(1) Dreaden, E.; Alkilany, A.; Huang, X.; Murphy, C.; El-Sayed, M. The Golden Age: Gold Nanoparticles for Biomedicine. *Chem. Soc. Rev.* **2012,** *41*, 2740-2779.
(2) DeVetter, B. M.; Sivapalan, S. T.; Patel, D. D.; Schulmerich, M. V.; Murphy, C. J.; Bhargava, R. Observation of Molecular Diffusion in Polyelectrolyte-Wrapped SERS Nanoprobes. *Langmuir* **2014,** *30*, 8931-8937.
(3) Schneider, G.; Decher, G.; Nerambourg, N.; Praho, R.; Werts, M. H. V.; Blanchard-Desce, M. Distance-Dependent Fluorescence Quenching on Gold Nanoparticles Ensheathed with Layer-by-Layer Assembled Polyelectrolytes. *Nano Lett.* **2006,** *6*, 530-536.
(4) Elbakry, A.; Zaky, A.; Liebkl, R.; Rachel, R.; Goepferich, A.; Breunig, M. Layer-by-Layer Assembled Gold Nanoparticles for siRNA Delivery. *Nano Lett.* **2009,** *9*, 2059-2064.
(5) Guo, S. T.; Huang, Y. Y.; Jiang, Q. A.; Sun, Y.; Deng, L. D.; Liang, Z. C.; Du, Q. A.; Xing, J. F.; Zhao, Y. L.; Wang, P. C.; et al. Enhanced Gene Delivery and siRNA Silencing by Gold Nanoparticles Coated with Charge-Reversal Polyelectrolyte. *ACS Nano* **2010,** *4*, 5505-5511.
(6) Chen, Q.; Bae, S. C.; Granick, S. Directed Self-Assembly of a Colloidal Kagome Lattice. *Nature* **2011,** *469*, 381-384.
(7) Ma, C.; Wu, H.; Huang, Z.-H.; Guo, R.-H.; Hu, M.-B.; Kubel, C.; Yan, L.-T.; Wang, W. A Filled-Honeycomb-Structured Crystal Formed by Self-Assembly of a Janus Polyoxometalate-Silsesquioxane (POM-POSS) Co-Cluster. *Angew. Chem.* **2015,** *54*, 15699-15704.

(8) Xu, G.; Huang, Z.; Chen, P.; Cui, T.; Zhang, X.; Miao, B.; Yan, L.-T. Optimal Reactivity and Improved Self-Healing Capability of Structurally Dynamic Polymers Grafted on Janus Nanoparticles Governed by Chain Stiffness and Spatial Organization. *Small* **2017,** *13*, 1603155.
(9) Maurer-Jones, M. A.; Gunsolus, I. L.; Murphy, C. J.; Haynes, C. L. Toxicity of Engineered Nanoparticles in the Environment. *Anal. Chem.* **2013,** *85*, 3036-3049.
(10) Murphy, C.; Vartanian, A.; Geiger, F.; Hamers, R.; Pedersen, R.; Cui, Q.; Haynes, C.; Carlson, E.; Hernandez, R.; Klaper, R.; et al. Biological Responses to Engineered Nanomaterials: Needs for the Next Decade. *ACS Cent. Sci.* **2015,** *1*, 117–123.
(11) Van Lehn, R. C.; Ricci, M.; Silva, P. H. J.; Andreozzi, P.; Reguera, J.; Voitchovsky, K.; Stellacci, F.; Alexander-Katz, A. Lipid Tail Protrusions Mediate the Insertion of Nanoparticles into Model Cell Membranes. *Nat. Commun.* **2014,** *5*, 1-11.
(12) Gkeka, P.; Angelikopoulos, P.; Sarkisov, L.; Cournia, Z. Membrane Partitioning of Anionic, Ligand-Coated Nanoparticles Is Accompanied by Ligand Snorkeling, Local Disordering, and Cholesterol Depletion. *PLoS Comput. Biol.* **2014,** *10*, e1004769.
(13) Heikkila, E.; Martinez-Seara, H.; Gurtovenko, A. A.; Javanainen, M.; Hakkinen, H.; Vattulainen, I.; Akola, J. Cationic Au Nanoparticle Binding with Plasma Membrane-like Lipid Bilayers: Potential Mechanism for Spontaneous Permeation to Cells Revealed by Atomistic Simulations. *J. Phys. Chem. C* **2014,** *118*, 11131-11141.
(14) Heikkila, E.; Martinez-Seara, H.; Gurtovenko, A. A.; Vattulainen, I.; Akola, J. Atomistic Simulations of Anionic $Au_{144}(SR)_{60}$ Nanoparticles Interacting with Asymmetric Model Lipid Membranes. *Biochim. Biophys. Acta* **2014,** *1838*, 2852-2860.
(15) Simonelli, F.; Bochicchio, D.; Ferrando, R.; Rossi, G. Monolayer-Protected Anionic Au Nanoparticles Walk into Lipid Membranes Step by Step. *J. Phys. Chem. Lett.* **2015,** *6*, 3175-3179.
(16) Feng, Z. V.; Gunsolus, I. L.; Qiu, T. A.; Hurley, K. R.; Nyberg, L. H.; Frew, H.; Johnson, K. P.; Vartanian, A. M.; Jacob, L. M.; Lohse, S. E.; et al. Impacts of Gold Nanoparticle Charge and Ligand Type on Surface Binding and Toxicity to Gram-Negative and Gram-Positive Bacteria. *Chem. Sci.* **2015,** *6*, 5186-5196.
(17) Troiano, J. M.; Olenick, L. L.; Kuech, T. R.; Melby, E. S.; Hu, D. H.; Lohse, S. E.; Mensch, A. C.; Dogangun, M.; Vartanian, A. M.; Torelli, M. D.; et al. Direct Probes of 4 nm Diameter Gold Nanoparticles Interacting with Supported Lipid Bilayers. *J. Phys. Chem. C* **2015,** *119*, 534-546.
(18) Dominguez, G. A.; Lohse, S. E.; Torelli, M. D.; Murphy, C. J.; Hamers, R. J.; Orr, G.; Klaper, R. D. Effects of Charge and Surface Ligand Properties of Nanoparticles on Oxidative Stress and Gene Expression within the Gut of *Daphnia magna*. *Aquat. Toxicol.* **2015,** *162*, 1-9.
(19) Qiu, T. A.; Bozich, J. S.; Lohse, S. E.; Vartanian, A. M.; Jacob, L. M.; Meyer, B. M.; Gunsolus, I. L.; Niemuth, N. J.; Murphy, C. J.; Haynes, C. L.; et al. Gene Expression as an Indicator of the Molecular Response and Toxicity in the Bacterium *Shewanella oneidensis* and the Water Flea *Daphnia magna* Exposed to Functionalized Gold Nanoparticles. *Environ. Sci.: Nano* **2015,** *2*, 615-629.
(20) Cui, Q.; Hernandez, R.; Mason, S. E.; Frauenheim, T.; Pedersen, J. A.; Geiger, F. Sustainable Nanotechnology: Opportunities and Challenges for Theoretical/Computational Studies. *J. Phys. Chem. B* **2016,** *120*, 7297-7306.
(21) Hernandez, R.; Popov, A. Molecular Dynamics Out of Equilibrium: Mechanics and Measurables. *Wiley Interdiscip. Rev. Comput. Mol. Sci.* **2014,** *4*, 541-561.

(22) Marrink, S. J.; de Vries, A. H.; Mark, A. E. Coarse Grained Model for Semiquantitative Lipid Simulations. *J. Phys. Chem. B* **2004,** *108*, 750-760.
(23) Marrink, S. J.; Risselada, H. J.; Yefimov, S.; Tieleman, D. P.; de Vries, A. H. The MARTINI Force Field: Coarse Grained Model for Biomolecular Simulations. *J. Phys. Chem. B* **2007,** *111*, 7812-7824.
(24) Lin, J.-Q.; Zhang, H.-W.; Chen, Z.; Zheng, Y.-G.; Zhang, Z.-Q.; Ye, H.-F. Simulation Study of Aggregations of Monolayer-Protected Gold Nanoparticles in Solvents. *J. Phys. Chem. C* **2011,** *115*, 18991-18998.
(25) da Rocha, E. L.; Caramori, G. F.; Rambo, C. R. Nanoparticle Translocation through a Lipid Bilayer Tuned by Surface Chemistry. *Phys. Chem. Chem. Phys.* **2013,** *15*, 2282-2290.
(26) Rossi, G.; Monticelli, L.; Puisto, S. R.; Vattulainen, I.; Ala-Nissila, T. Coarse-Graining Polymers with the MARTINI Force-Field: Polystyrene as a Benchmark Case. *Soft Matter* **2011,** *7*, 698-708.
(27) Patel, P. A.; Jeon, J.; Mather, P. T.; Dobrynin, A. V. Molecular Dynamics Simulations of Layer-by-Layer Assembly of Polyelectrolytes at Charged Surfaces: Effects of Chain Degree of Polymerization and Fraction of Charged Monomers. *Langmuir* **2005,** *21*, 6113-6122.
(28) Panchagnula, V.; Jeon, J.; Dobrynin, A. V. Molecular Dynamics Simulations of Electrostatic Layer-by-Layer Self-Assembly. *Phys. Rev. Lett.* **2004,** *93*, 037801.
(29) Carnal, F.; Stoll, S. Adsorption of Weak Polyelectrolytes on Charged Nanoparticles. Impact of Salt Valency, pH, and Nanoparticle Charge Density. Monte Carlo Simulations. *J. Phys. Chem. B* **2011,** *115*, 12007-12018.
(30) Zhang, Y. Q.; Fry, C. G.; Pedersen, J. A.; Hamers, R. J. Dynamics and Morphology of Nanoparticle-Linked Polymers Elucidated by Nuclear Magnetic Resonance. *Anal. Chem.* **2017,** *89*, 12399-12407.
(31) Troiano, J. M.; Kuech, T. R.; Vartanian, A. M.; Torelli, M. D.; Sen, A.; Jacob, L. M.; Hamers, R. J.; Murphy, C. J.; Pedersen, J. A.; Geiger, F. M. On Electronic and Charge Interference in Second Harmonic Generation Responses from Gold Metal Nanoparticles at Supported Lipid Bilayers. *J. Phys. Chem. C* **2016,** *120*, 20659-20667.
(32) Park, J. W.; Shumaker-Parry, J. S. Structural Study of Citrate Layers on Gold Nanoparticles: Role of Intermolecular Interactions in Stabilizing Nanoparticles. *J. Am. Chem. Soc.* **2014,** *136*, 1907-1921.
(33) Mdluli, P. S.; Sosibo, N. M.; Mashazi, P. N.; Nyokong, T.; Tshikhudo, R. T.; Skepu, A.; van der Lingen, E. Selective Adsorption of PVP on the Surface of Silver Nanoparticles: A Molecular Dynamics Study. *J. Mol. Struct.* **2011,** *1004*, 131-137.
(34) Kyrychenko, A.; Korsun, O. M.; Gubin, I. I.; Kovalenko, S. M.; Kalugin, O. N. Atomistic Simulations of Coating of Silver Nanoparticles with Poly(vinylpyrrolidone) Oligomers: Effect of Oligomer Chain Length. *J. Phys. Chem. C* **2015,** *119*, 7888-7899.
(35) Suh, J.; Paik, H.-J.; Hwang, B. K. Ionization of Poly(ethylenimine) and Poly(allylamine) at Various pH's. *Bioorg. Chem.* **1994,** *22*, 318-327.
(36) Troiano, J. M.; McGeachy, A. C.; Olenick, L. L.; Fang, D.; Liang, D. Y.; Hong, J. W.; Kuech, T. R.; Caudil, E. R.; Pedersen, J. A.; Cui, Q.; et al. Quantifying the Electrostatics of Polycation-Lipid Bilayer Interactions. *J. Am. Chem. Soc.* **2017,** *139*, 5808-5816.
(37) Heinz, H.; Vaia, R. A.; Farmer, B. L.; Naik, R. R. Accurate Simulation of Surfaces and Interfaces of Face-Centered Cubic Metals Using 12-6 and 9-6 Lennard-Jones Potentials. *J. Phys. Chem. C* **2008,** *112*, 17281-17290.

(38) Ghorai, P. K.; Glotzer, S. C. Molecular Dynamics Simulation Study of Self-Assembled Monolayers of Alkanethiol Surfactants on Spherical Gold Nanoparticles. *J. Phys. Chem. C* **2007,** *111*, 15857-15862.
(39) Ahn, Y.; Saha, J. K.; Schatz, G. C.; Jang, J. Molecular Dynamics Study of the Formation of a Self-Assembled Monolayer on Gold. *J. Phys. Chem. C* **2011,** *115*, 10668-10674.
(40) Jorgensen, W. L.; Madura, J. D.; Swenson, C. J. Optimized Intermolecular Potential Functions for Liquid Hydrocarbons. *J. Am. Chem. Soc.* **1984,** *106*, 6638-6646.
(41) Jorgensen, W. L.; Maxwell, D. S.; Tirado-Rives, J. Development and Testing of the OPLS All-Atom Force Field on Conformational Energetics and Properties of Organic Liquids. *J. Am. Chem. Soc.* **1996,** *118*, 11225-11236.
(42) Brancolini, G.; Corazza, A.; Vuano, M.; Fogolari, F.; Mimmi, M. C.; Bellotti, V.; Stoppini, M.; Corni, S.; Esposito, G. Probing the Influence of Citrate-Capped Gold Nanoparticles on an Amyloidogenic Protein. *ACS Nano* **2015,** *9*, 2600-2613.
(43) Wright, L. B.; Rodger, P. M.; Walsh, T. R. Aqueous Citrate: A First-Principles and Force-Field Molecular Dynamics Study. *RSC Adv.* **2013,** *3*, 16399-16409.
(44) Kostritskii, A. Y.; Kondinskaia, D. A.; Nesterenko, A. M.; Gurtovenko, A. A. Adsorption of Synthetic Cationic Polymers on Model Phospholipid Membranes: Insight from Atomic-Scale Molecular Dynamics Simulations. *Langmuir* **2016,** *32*, 10402-10414.
(45) Lin, W.; Insley, T.; Tuttle, M. D.; Zhu, L. Y.; Berthold, D. A.; Kral, P.; Rienstra, C. M.; Murphy, C. J. Control of Protein Orientation on Gold Nanoparticles. *J. Phys. Chem. C* **2015,** *119*, 21035-21043.
(46) Chang, R. W.; Yethiraj, A. Dilute Solutions of Strongly Charged Flexible Polyelectrolytes in Poor Solvents: Molecular Dynamics Simulations with Explicit Solvent. *Macromolecules* **2006,** *39*, 821-828.
(47) Martinez, L.; Andrade, R.; Birgin, E. G.; Martinez, J. M. Packmol: A Package for Building Initial Configurations for Molecular Dynamics Simulations. *J. Comput. Chem.* **2009,** *30*, 2157-2164.
(48) Plimpton, S. Fast Parallel Algorithms for Short-Range Molecular-Dynamics. *J. Comput. Phys.* **1995,** *117*, 1-19.
(49) Bureau, H.; Merz, D.; Hershkovits, E.; Quirk, S.; Hernandez, R. Constrained Unfolding of a Helical Peptide: Implicit versus Explicit Solvents. *PLoS One* **2015,** *10*, e0127034.
(50) Hoda, N.; Larson, R. G. Explicit- and Implicit-Solvent Molecular Dynamics Simulations of Complex Formation between Polycations and Polyanions. *Macromolecules* **2009,** *42*, 8851-8863.
(51) Reddy, G.; Yethiraj, A. Implicit and Explicit Solvent Models for the Simulation of Dilute Polymer Solutions. *Macromolecules* **2006,** *39*, 8536-8542.
(52) Reddy, G.; Yethiraj, A. Solvent Effects in Polyelectrolyte Adsorption: Computer Simulations with Explicit and Implicit Solvent. *J. Chem. Phys.* **2010,** *132*, 074903.
(53) Hoogerbrugge, P.; Koelman, J. Simulating Microscopic Hydrodynamic Phenomena with Dissipative Particle Dynamics. *Europhys. Lett.* **1992,** *19*, 155-160.
(54) Groot, R. D.; Warren, P. B. Dissipative Particle Dynamics: Bridging the Gap between Atomistic and Mesoscopic Simulation. *J. Chem. Phys.* **1997,** *107*, 4423-4435.
(55) Qiu, T. A.; Torelli, M. D.; Vartanian, A. M.; Rackstraw, N. B.; Buchman, J. T.; Jacob, L. M.; Murphy, C. J.; Hamers, R. J.; Haynes, C. L. Quantification of Free Polyelectrolytes Present in Colloidal Suspension, Revealing a Source of Toxic Responses for Polyelectrolyte-Wrapped Gold Nanoparticles. *Anal. Chem.* **2017,** *89*, 1823-1830.

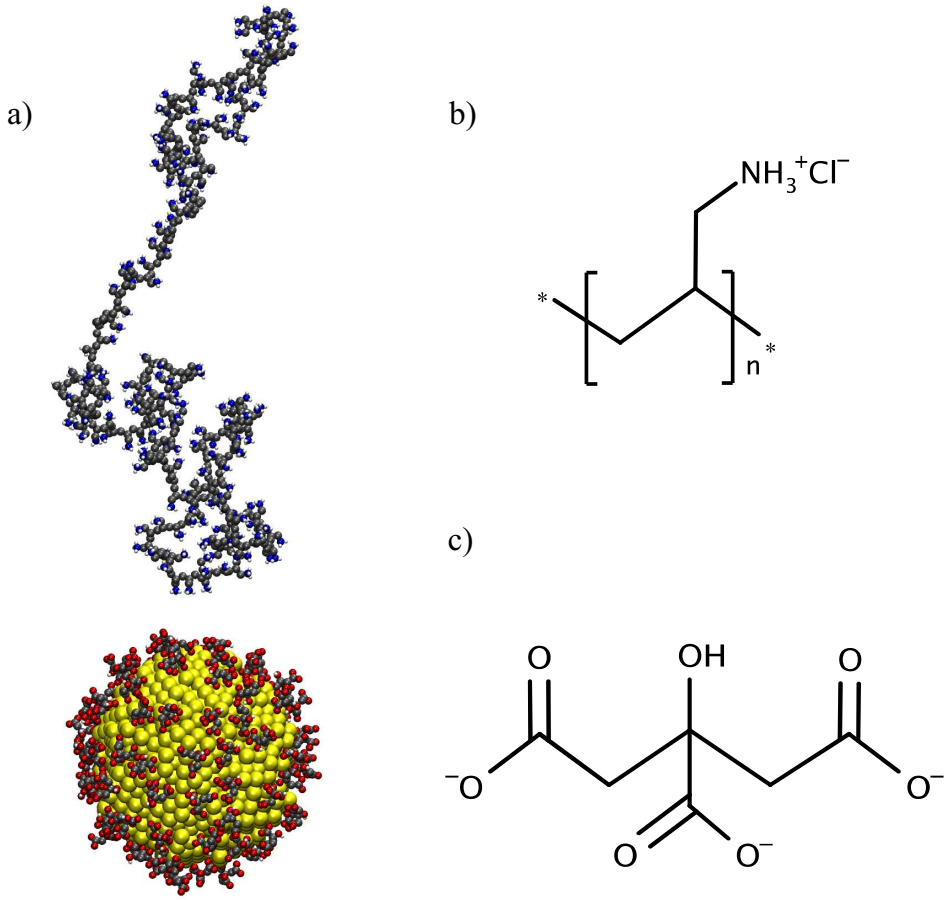

Figure 1. Representative structures for (a) the initial configuration for PAH_{200} deposition on citrate-coated AuNPs with gold (yellow), carbon (gray), oxygen (red), hydrogen (white), and nitrogen (blue) atoms (and counterions not shown for clarity); (b) a PAH monomer and (c) $citrate^{3-}$.

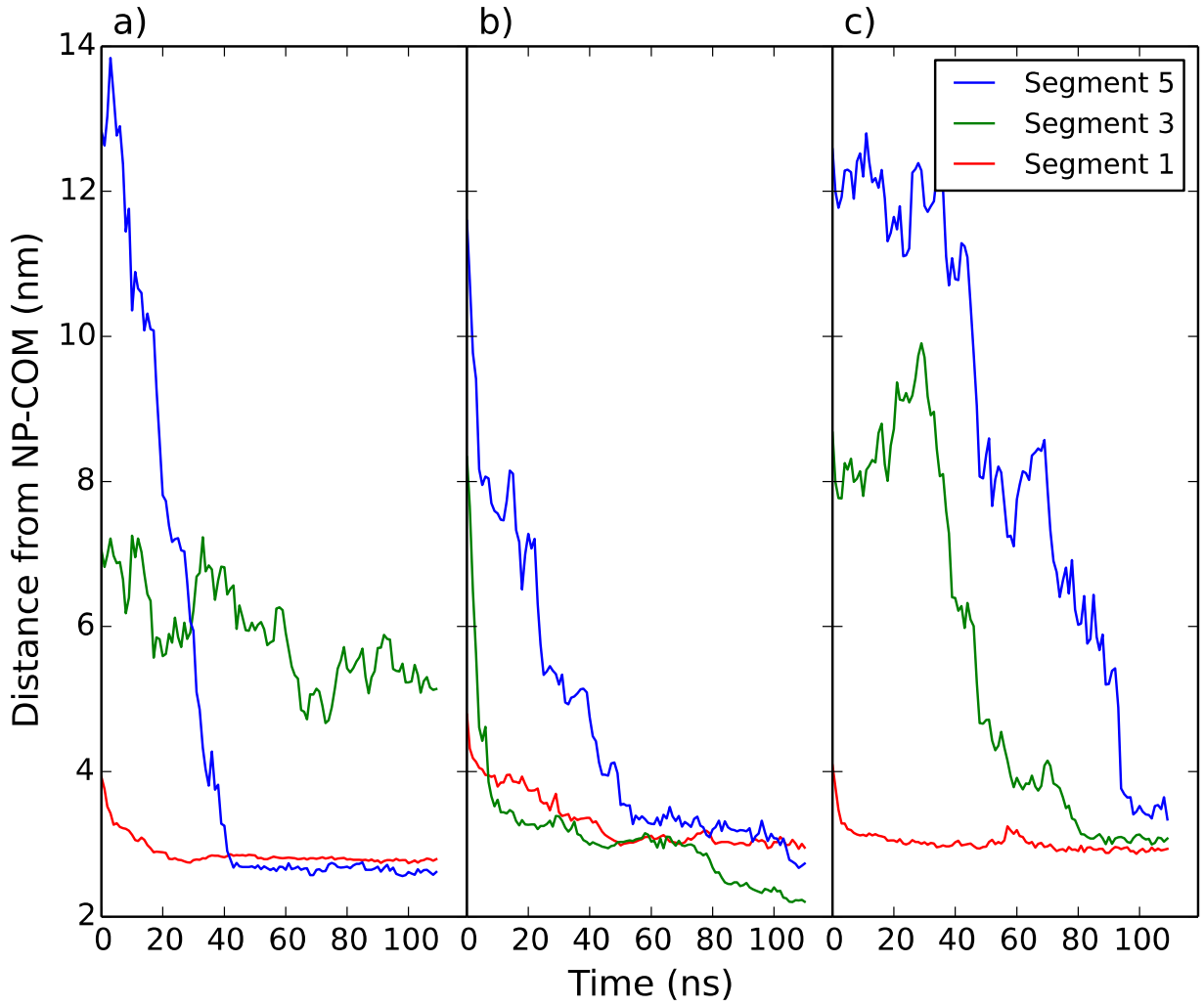

Figure 2. Adsorption of the center of mass of the 1st (Segment 1), 3rd (Segment 3), and 5th (Segment 5) 40-monomer segment of PAH_{200} over time in explicit solvent relative to the nanoparticle center of mass (NP-COM) for different PAH_{200} (a-c).

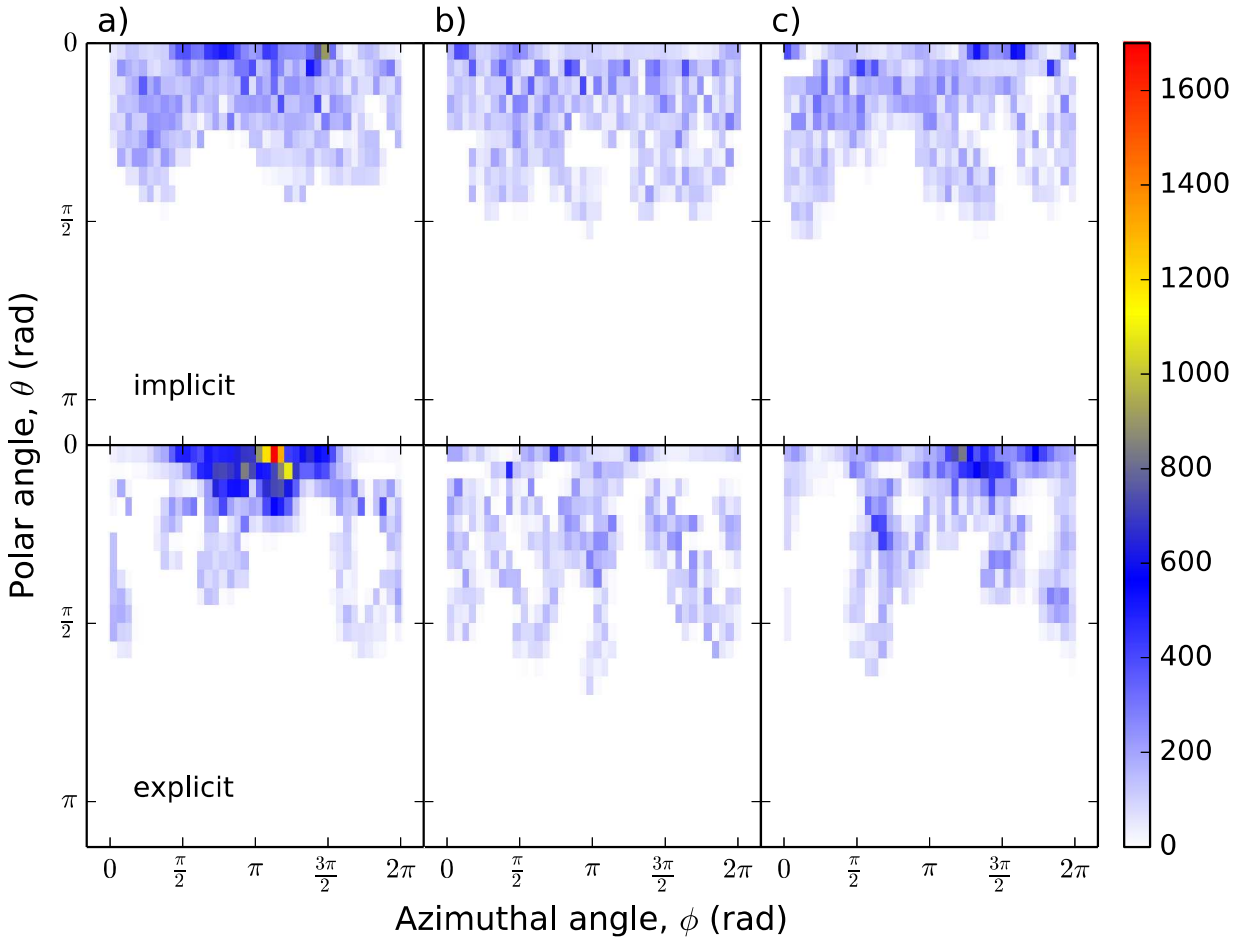

Figure 3. Surface coverage of nitrogen atoms of different PAH_{200} (a-c) in implicit and explicit solvent. The azimuthal angle ranges from 0 to 2π radians along the equator of the nanoparticle. The polar angle ranges from 0 radians at the north pole to π radians at the south pole. The bin size of the two-dimensional histogram is π/20 radians. The color scale shows the density of the nitrogen atoms.

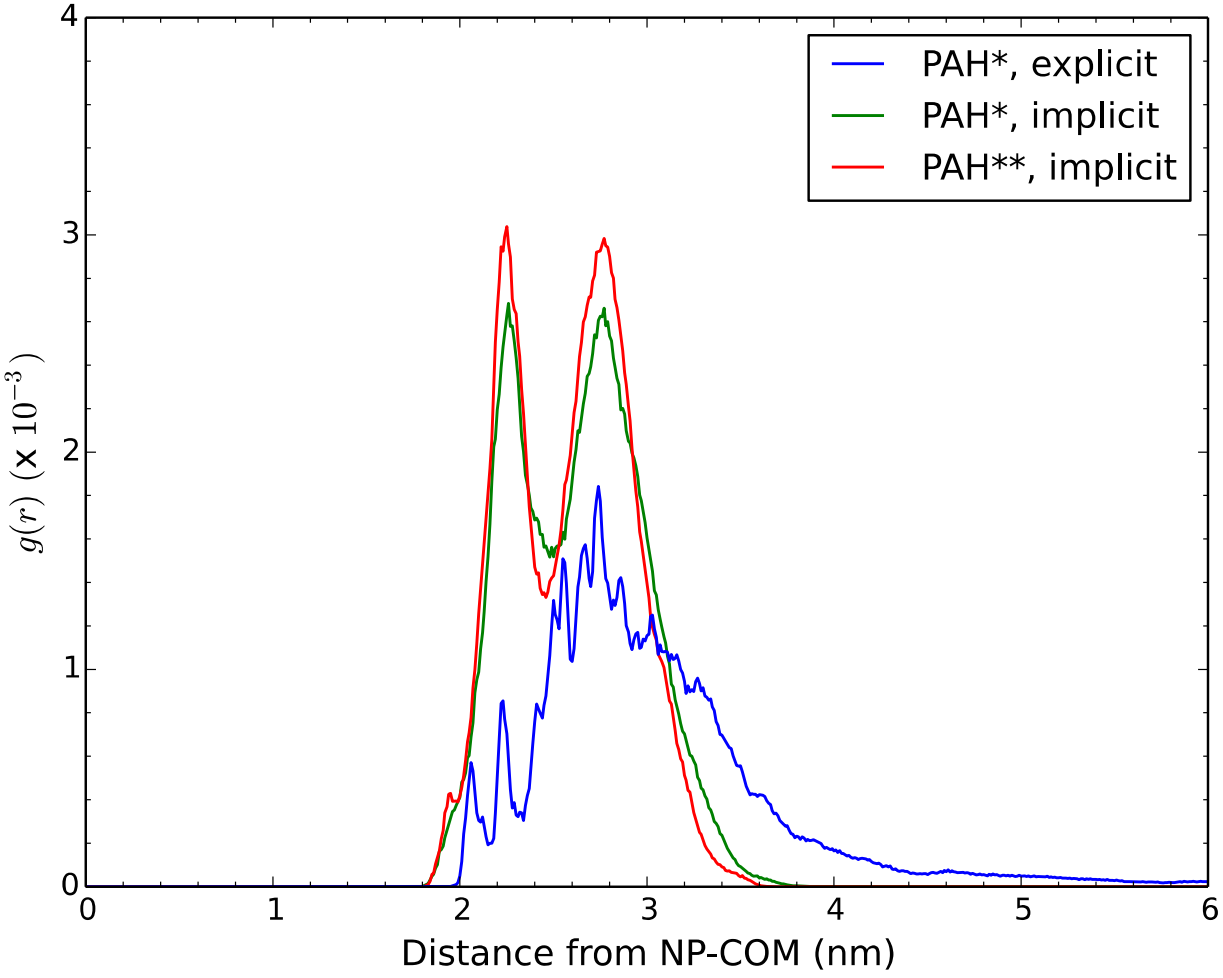

Figure 4. Radial distribution function, *g(r)*, between the nitrogen atoms of PAH_{200} deposited on the upper hemisphere of a nanoparticle and the nanoparticle center of mass (NP-COM). The asterisk (*) denotes the number of PAH_{200} added to the nanoparticle. For **, a second PAH_{200} was deposited on the bottom hemisphere of the AuNP.

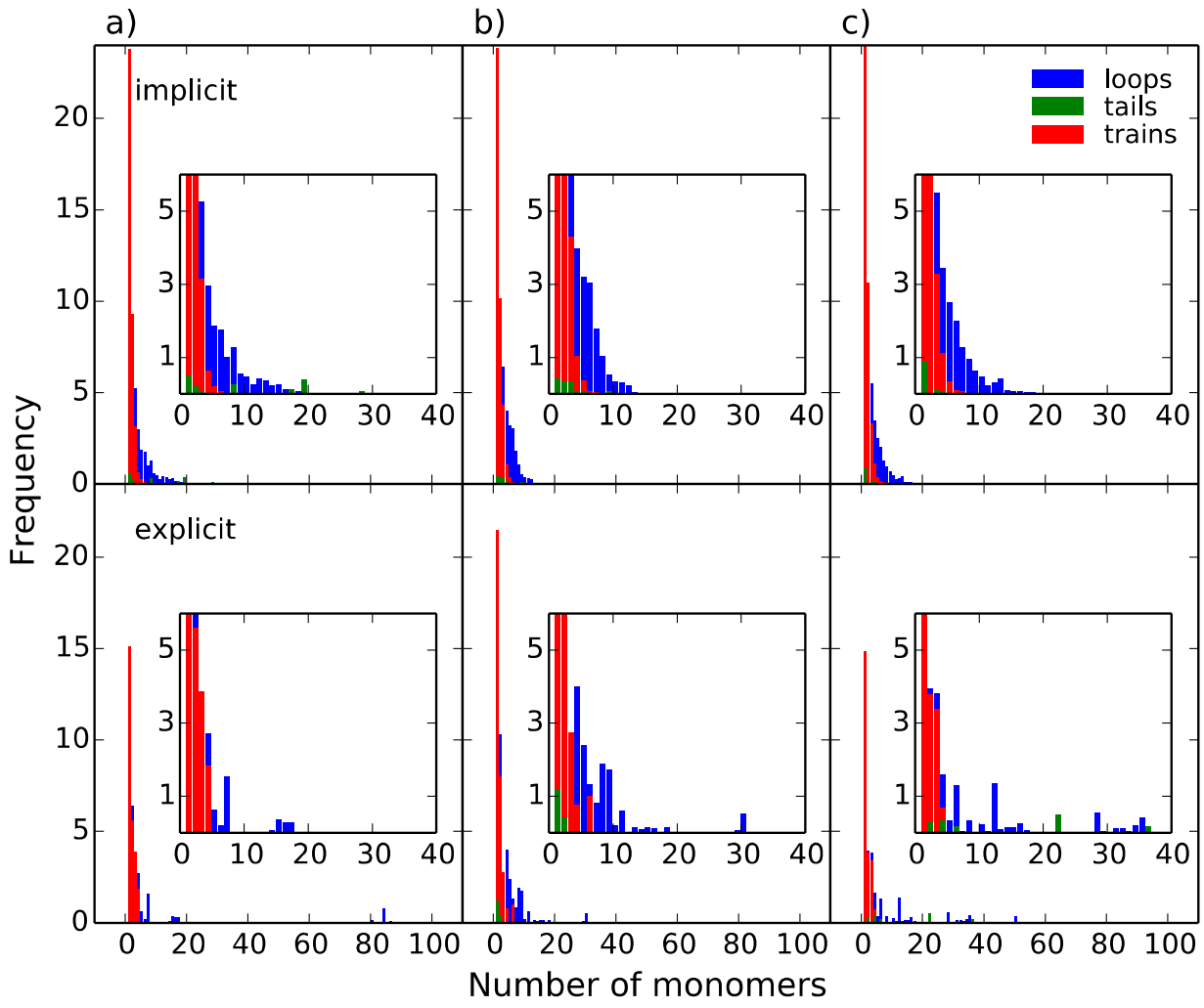

Figure 5. Histogram of the frequency of solvent-exposed loops, free tails, and surface-bound trains with *n* number of monomers within different PAH_{200} (a-c) in implicit and explicit solvent. The distributions are divided by the total number of frames sampled such that 1.0 indicates one instance in every frame.

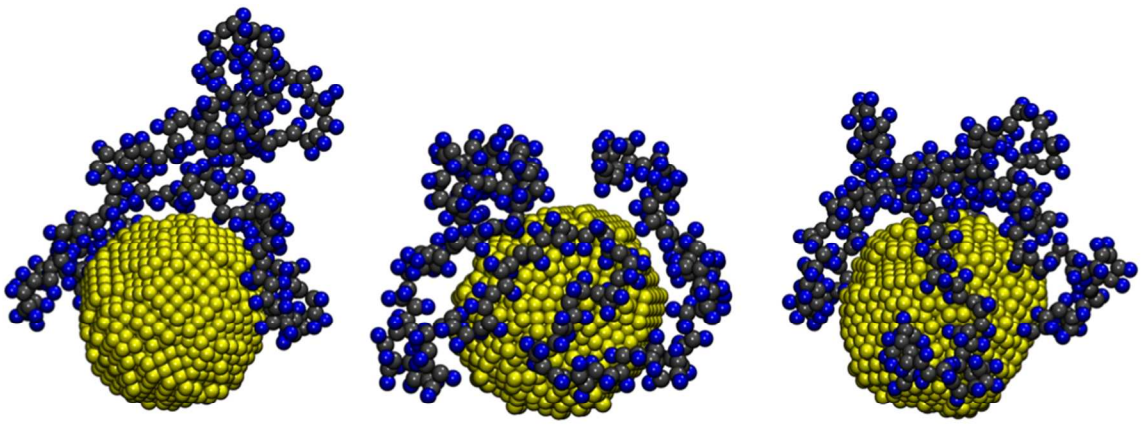

Figure 6. PAH_{200} models coarse-grained per monomer by the center of mass of the carbon atoms (gray) and of the NH_3^+ group (blue) on an atomistic 4-nm gold core.

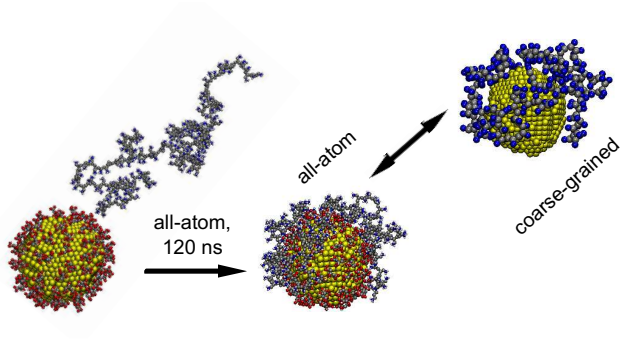

TOC Graphic

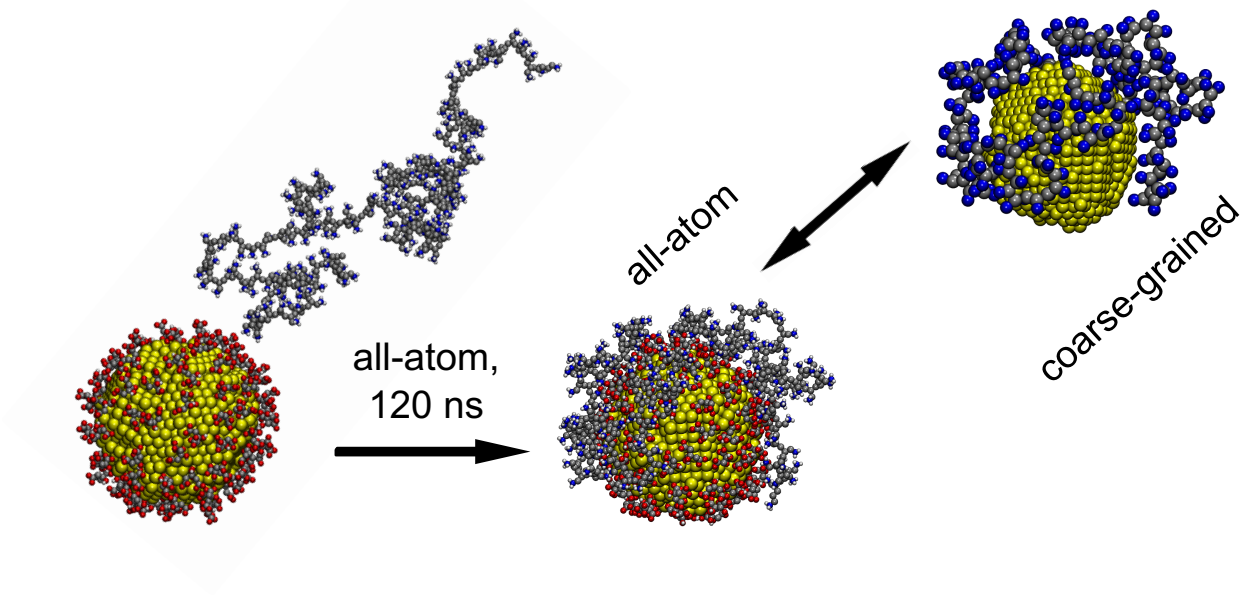
all-atom,
120 ns
all-atom
coarse-grained

a)

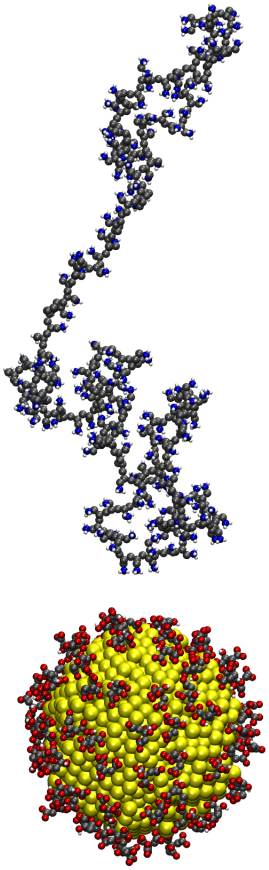

b)

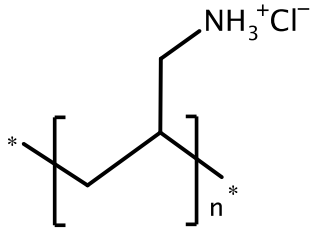

c)

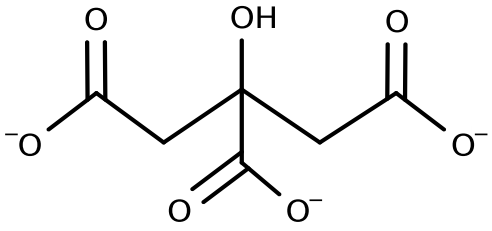

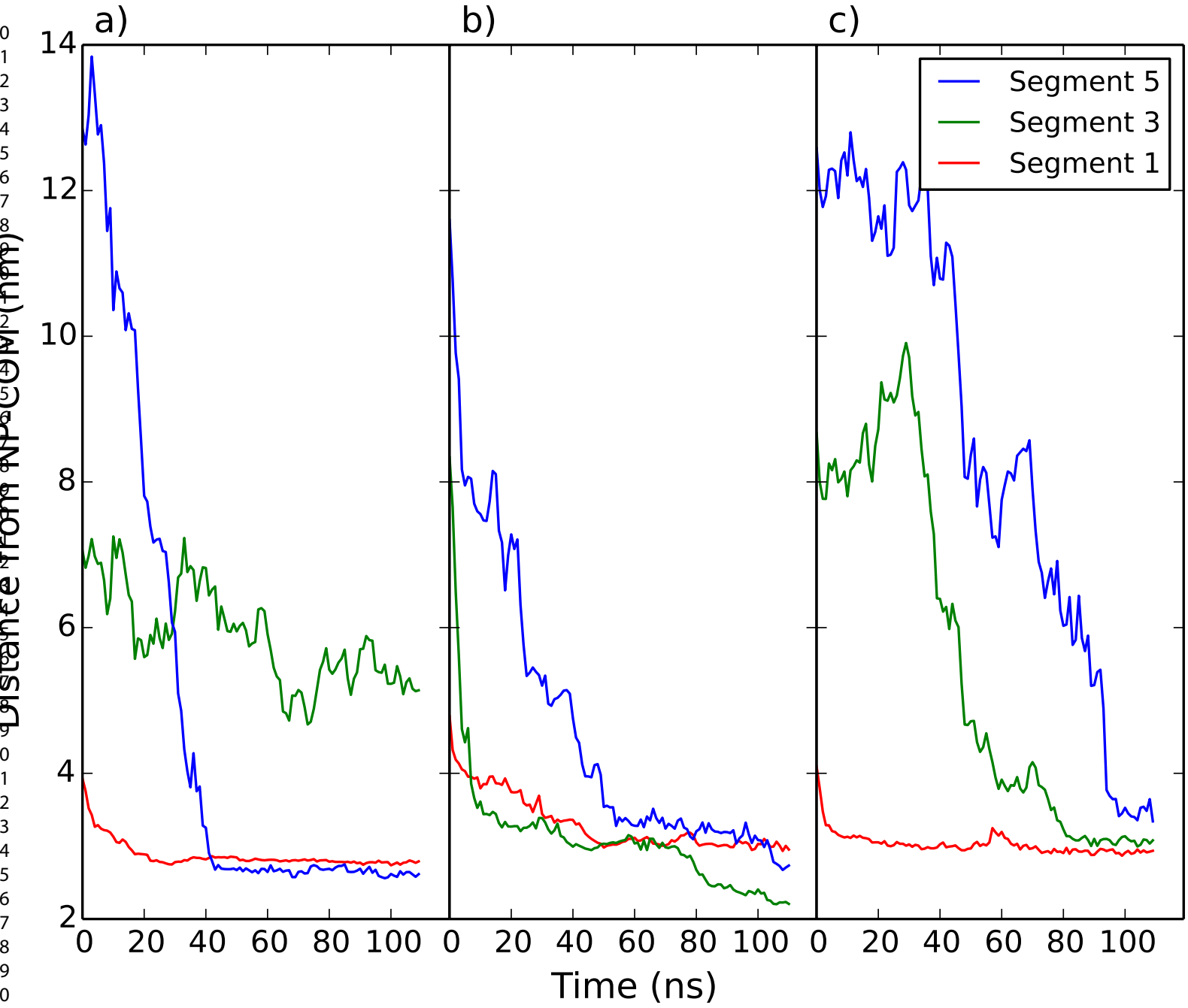
a)
b)
c)
Segment 5
Segment 3
Segment 1
Distance from NP COM (nm)
Time (ns)
2
4
6
8
10
12
14
0
20
40
60
80
100

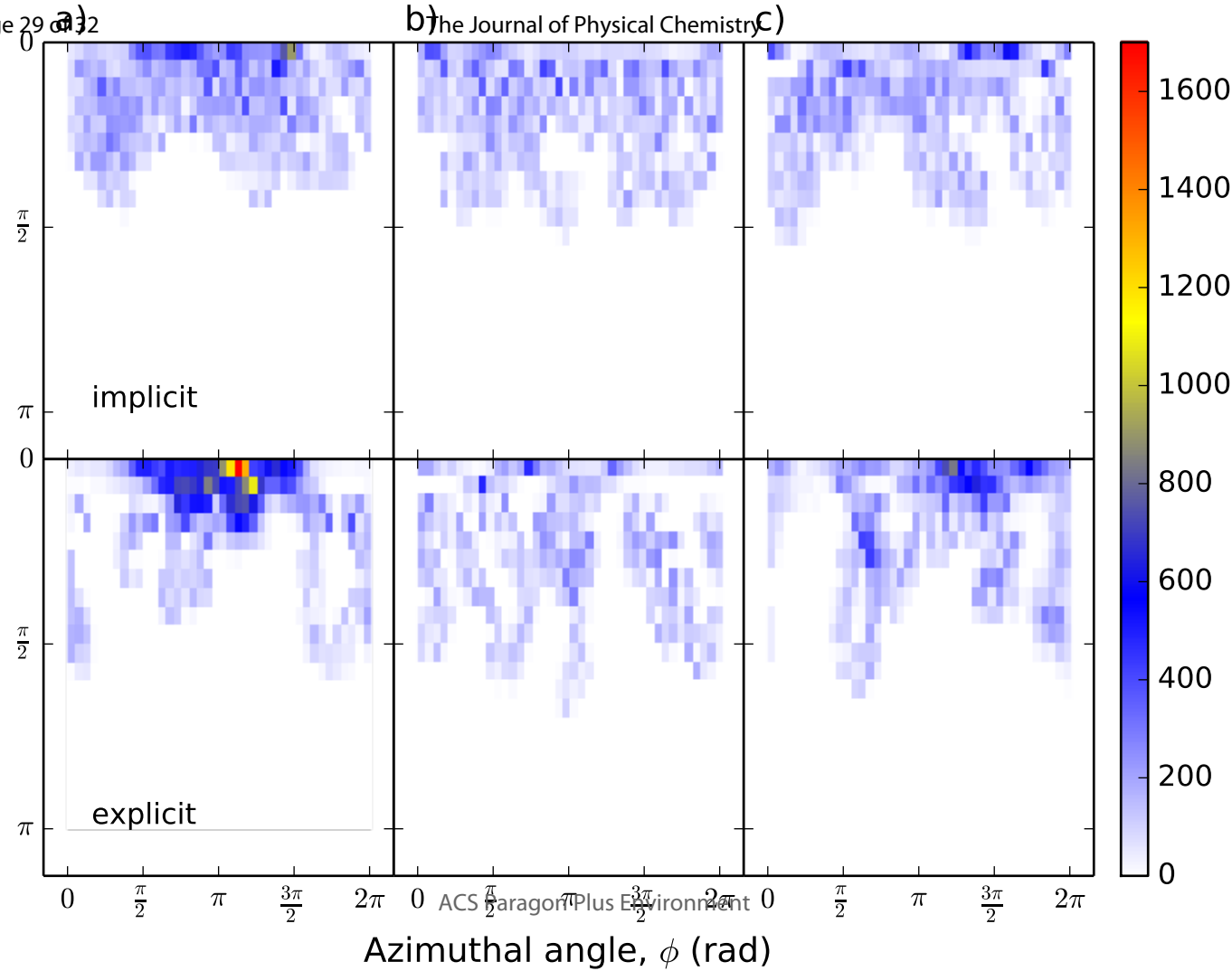

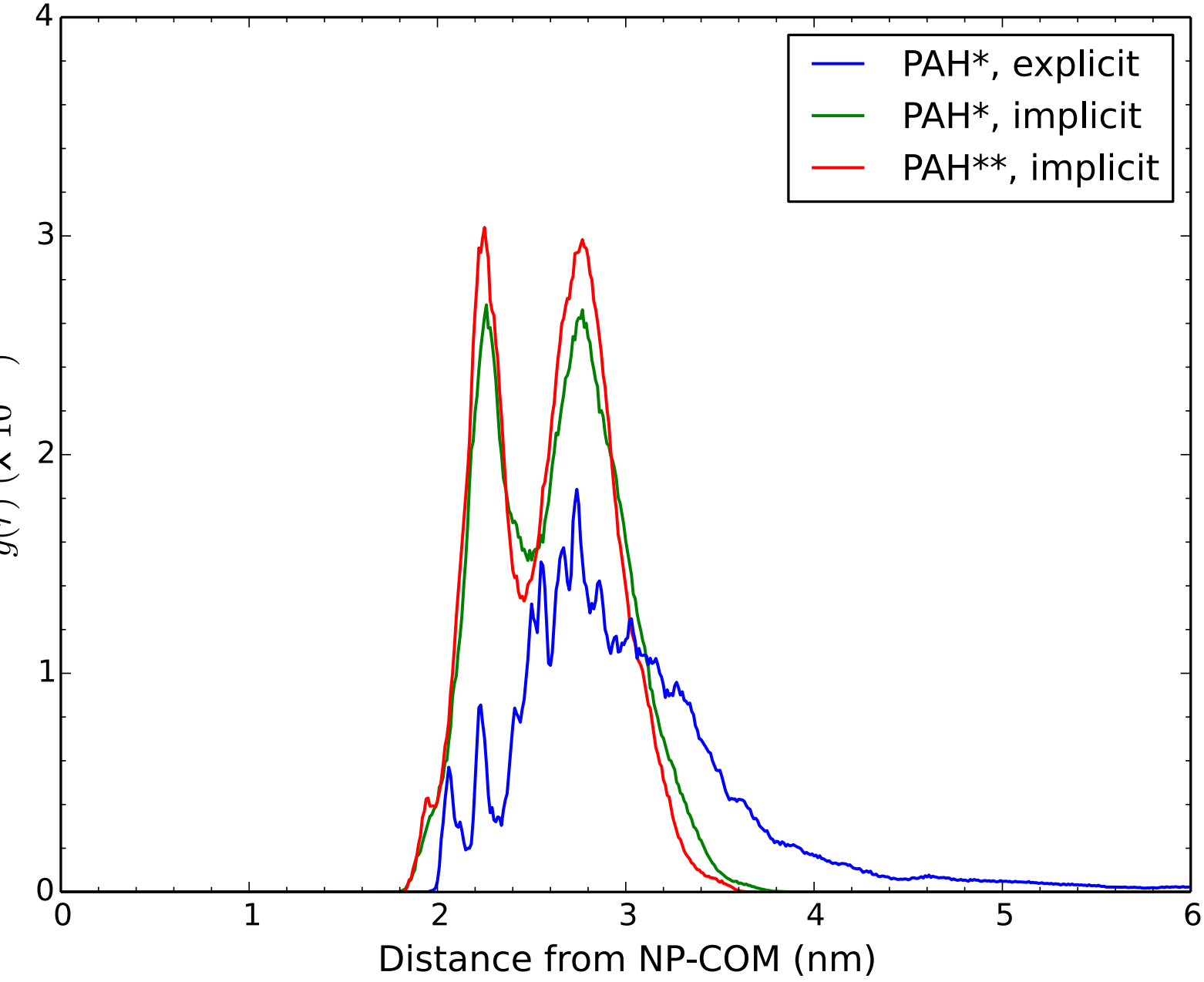
PAH*, explicit
PAH*, implicit
PAH**, implicit
$g(r)$ ($\times 10^{-3}$)
Distance from NP-COM (nm)
0
1
2
3
4
5
6

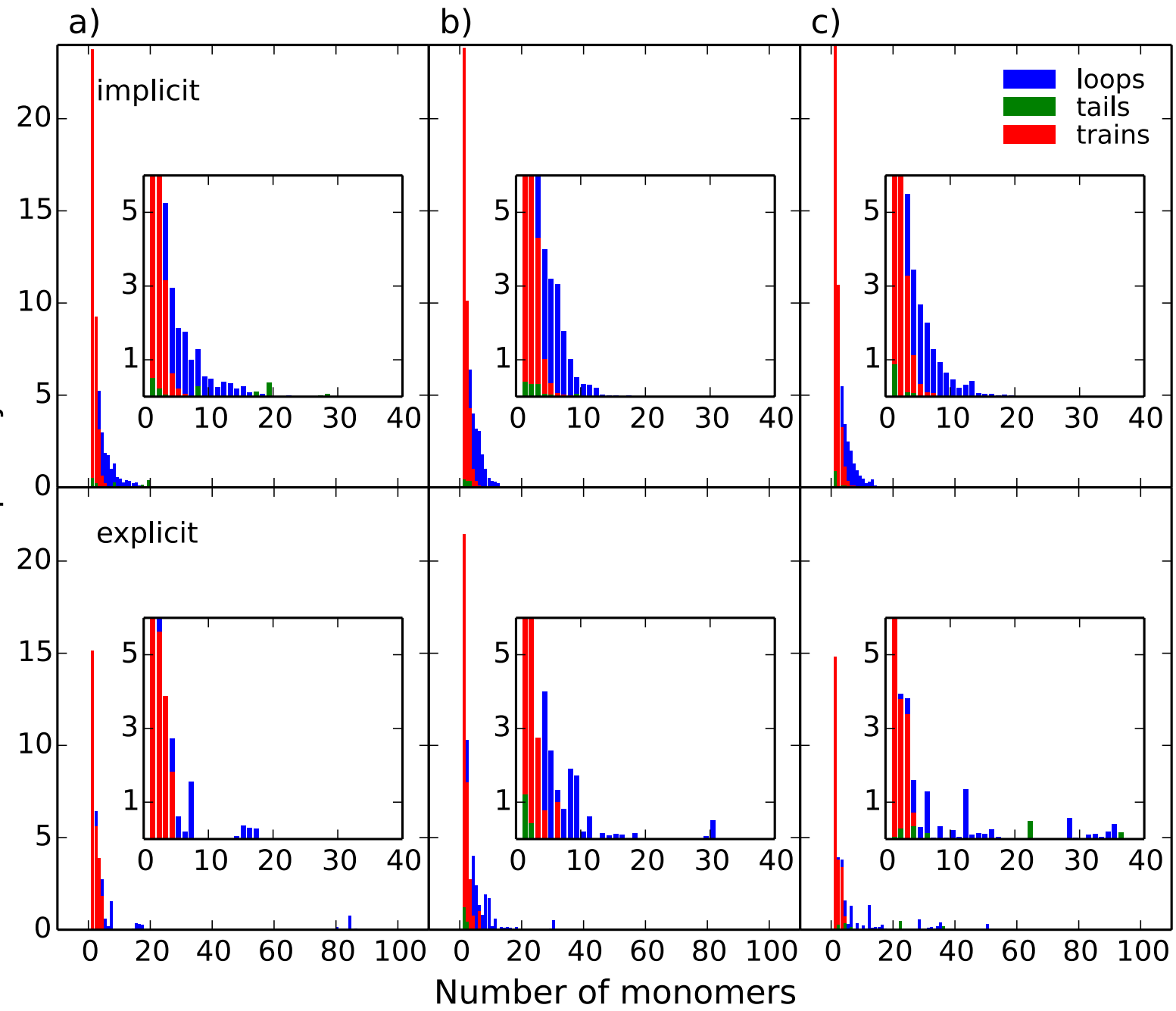
a)
b)
c)
implicit
explicit
loops
tails
trains
Frequency
Number of monomers